Fabrication of Epitaxial Thin Films by Pulsed Laser Deposition and Structural Studies of $(Ba_{0.85}Ca_{0.15})(Zr_{0.10}Ti_{0.90})O_3$: a Lead Free Piezoelectric

by

MuditUpadhyay

Supervisor

Dr. Ranjith Ramadurai

A Dissertation Submitted to

Indian Institute of Technology Hyderabad

In Partial Fulfillment of the Requirements for

The Degree of Master of Technology

भारतीय प्रौद्योगिकी संस्थान हैदराबाद
Indian Institute of Technology Hyderabad

Department of Materials Science and Metallurgical Engineering

June, 2015

Declaration

I declare that this written submission represents my ideas in my own words, and where others' ideas or words have been included, I have adequately cited and referenced the original sources. I also declare that I have adhered to all principles of academic honesty and integrity and have not misrepresented or fabricated or falsified any idea/data/fact/source in my submission. I understand that any violation of the above will be a cause for disciplinary action by the Institute and can also evoke penal action from the sources that have thus not been properly cited, or from whom proper permission has not been taken when needed.

Mudit

Mudit Upadhyay

Ms13m1006

Approval Sheet

This thesis entitled "**Fabrication of Epitaxial Thin Films by Pulsed Laser Ablation and Structural Studies of** $(Ba_{0.85}Ca_{0.15})(Zr_{0.10}Ti_{0.90})O_3$ **: a Lead Free Piezoelectric**" by Mudit Upadhyay is approved for the degree of Master of Technology from IIT Hyderabad.

_____

Dr. Prem Pal

Associate Professor

Department of Physics

Examiner

_____

Dr. Subhradeep Chatterjee

Assistant Professor

Department of Materials Science and Metallurgical Engineering

Examiner

_____

Dr. Ranjith Ramadurai

Assistant Professor

Department of Materials Science and Metallurgical Engineering

Adviser

_____

Dr. Saswata Bhattacharya

Assistant Professor

Department of Materials Science and Metallurgical Engineering

Chairman

iii

Acknowledgements

First of all I would like to thank my guide Dr. Ranjith Ramadurai for his guidance, advices, and tremendous help during the project. Whenever I was depressed and tensed his constant encouragement helped me a lot throughout the year. Without his support and motivation I would not have completed it.

When I joined the Department of Materials Science and Metallurgical Engineering, I was completely new to the subject but lectures of all the faculty members helped me to build up my basic knowledge of the subject, I am very thankful to all of them.

I also want to thank all the Phd scholars of the department specially Mr. Mallesh, Mr. Saj Mohan, Mr. Kumar Swammy and Mr. Venkat for helping me to complete my experiments, for sharing their knowledge with me and also for listening my boring mock presentations and giving me lot of suggestions to improve it further.

I would also like to acknowledge Dr. Adhiraj Srinivas (Scientist E, DMRL) and Mr. K. Prabahar (Scientist B, DMRL) for allowing me to use their laboratory for preparation of my sample.

My parents and siblings have not seen much of me during the last two years, but their constant support and love was always there for me. I cannot tell how much grateful I am towards all of you.

Last but not the least, life in IIT Hyderabad would have been very boring if I did not have my dear and crazy friends. Thank you very much guys for making last two years memorable and thank you very much for all the support during my project work.

Dedicated to

My Parents

Abstract

After the discovery of piezoelectricity in 1880 by Curie brothers, the drive for basic science behind the phenomenon and utilization for new applications begun. Later the discovery of PZT (Lead Zirconate Titanate) led to saturation in further discoveries because of its superior piezoelectric properties. But the presence of lead in PZT is known to be hazardous to the environment. Hence, the need for lead free piezoelectric materials arose. In 2009 *Wenfeng Liu* reported high dielectric constant value in lead free piezoelectric materials $Ba_{0.85}Ca_{0.15}Zr_{0.10}Ti_{0.90}O_3$(BCZT). The basic approach to achieving high piezoelectricity is to place the composition of the material to the proximity of a composition-induced phase transition between two ferroelectric phases. Easy domain switching with low energy barrier was the reason for high piezoelectric constants values in BCZT. Later BCZT has been extensively studied in bulk but the field of BCZT thin films still needs to be studied for both fundamental aspects and applications. .

This projects aims in addressing the issue on growth of epitaxial thin films of BCZT using pulsed laser ablation technique. Initially, BCZT pellet was prepared with the solid state reaction route followed by the deposition of BCZT on $SrTiO_3$ (001) substrate using Pulsed Laser Deposition (PLD) technique. As substrate quality plays an important role in the quality of thin films, various methodologies have been adopted to obtain stepped substrate surface. The quality of thin films was characterized using High Resolution X-Ray Diffraction (HRXRD) and Atomic Force Microscopy (AFM). Epitaxial growth was obtained which was matching with the substrate orientation as confirmed by RSM (Reciprocal Space Mapping). It was found that for depositing the epitaxial films of BCZT the substrate temperature plays a very important role. Hence, we report the role of substrate temperature on the growth of BCZT epitaxial thin films. The films deposited at $650^{o}C$ show complete strain relaxation and possessed better morphology in comparison to films grown at other temperatures.

Contents

Chapter 1

Introduction

"Ability of a material to generate electricity on application of pressure"

Interesting story of sensors, actuators and transducers started with the discovery of direct piezoelectric effectin single crystal quartz by Curie brothers (Pierre and Jacques Curie) in 1880 [1]. Later in 1881 Mr.Gabriel Lippmann discovered the reverse piezoelectric effect. Later in 1914 during World War I, Dr. Paul Langevin developed the first ultrasonic transducer using piezoelectric effect of quartz single crystal, contemporarily there were other piezoelectrics were also discovered; like Rochelle salt ($NaKC_4H_4O_6.4H_2O$), Potassium Dihydrogen Phosphate (KDP), Poly vinylenedifluoride (PVDF). During World War II the necessity of water insoluble piezoelectric led to the discovery of $BaTiO_3$like ceramics. Consequently the discovery of PZT (Lead Zirconate) led tothe saturation in piezoelectric discoveries with its superior properties. But the hunt for lead free piezoelectric materials, drove the search for novel piezoelectrics,and since 1999 wide range of piezoelectric materials have been developed such as Bi-layered compounds, $(Na,K)NbO_3$, $(Bi_{0.5}Na_{0.5})TiO_3$ etc.[1]

1.1 Piezoelectricity:

Piezoelectricity could be understood as the linear interaction between mechanical and electrical energy in non-centric crystals.

Direct piezo effect: generation of electric field on application of mechanical stress is termed as direct piezo effect. Fig.1.1 (a)

Reverse piezo effect: generation of stress in a crystal on application of electric field is termed as reverse piezo effect. Fig.1.1 (b)

This phenomenon can be observed in crystal having no center-of-symmetry and prominently observed in crystals having perovskite structures (ABO_3). Most of the well-known piezoelectric materials like $BaTiO_3$, $PbTiO_3$ possess perovskite structures.
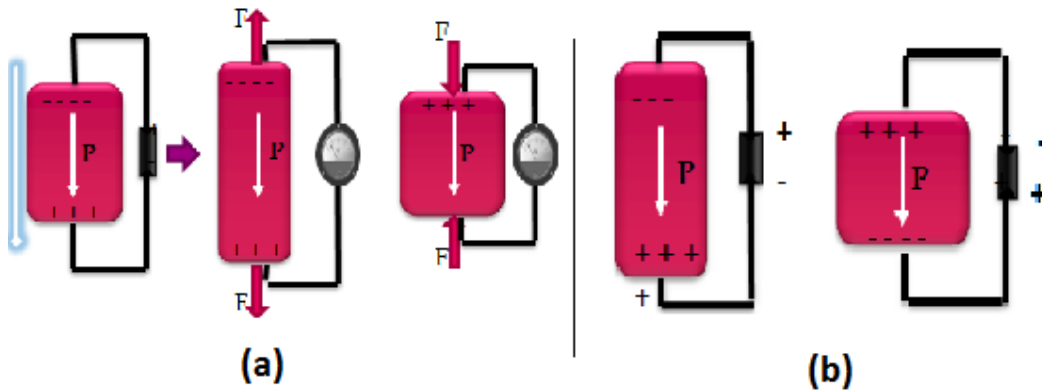

Fig 1.1*(a) Direct piezo effect(b) Reverse piezo effect[2]*

Some of the piezoelectric materials also have ferroelectric character with an extra ability to have the electric dipoles in adjacent unit cells interact with one another in such a way that the adjacent dipoles tend to align themselves.

1.2   Piezoelectricity in perovskite structure:

The commonly known group of piezoelectric materials is the perovskite (ABO_3) structure. The structure possess unit cell with Acations at cube corners, O^{-2} ions at face centers and Bcationson body center. The BO_6octahedra present at the center of the unit cell is responsible for the piezoelectric and ferroelectric properties of majority of the perovskites. On application of external mechanical stress, distortion in oxygen octahedra takes place and Bcation displaces from its center position. This distortion associated with the displacement of B cation reduces the symmetry and effectively giving rise to a net dipole moment and eventually the crystal becomes electrically polarized. This polarization generates electricity in the system. Some of the piezoelectricperovskiteexhibitswitchablespontaneous polarization below the Curie temperature, due to the homo-polar nature of the B – O bond in BO_6 octahedra. A closer binding between the B^{+4}ion and three of the O^{2-} ions causes the rattling nature of Bcations in the octahedra. This rattling results in the ferroelectric behavior of the perovskite structures like $BaTiO_3$[2]. Some of the examples of perovskite piezoelectric materials are – $BaTiO_3$, $PbTiO_3$, $LiNbO_3$ etc. Fig.1.2 shows the perovskite structure and the rattling nature of Bcation in the oxygen octahedra.
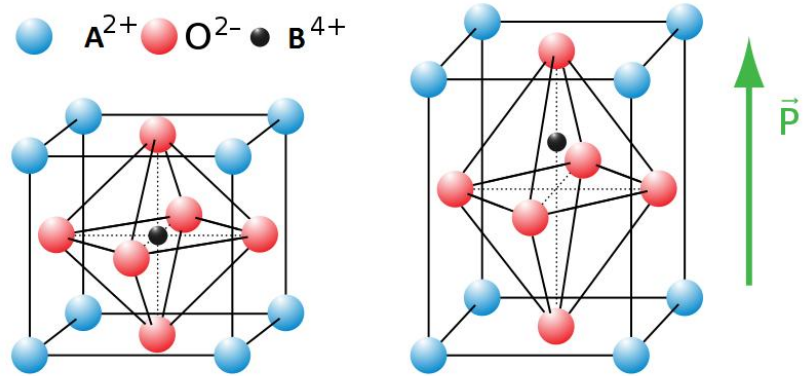
Fig 1.2 *(a) Perovskite structure, (b) Rattling nature of Bcatio in oxygen octahedr*a[3]

1.3 Piezoelectric constants:

(i) Piezoelectric strain constant (d):

The tensor that defines the coupling between external electric field and the strain, is called piezoelectric strain constant. Since piezoelectricity is an anisotropic phenomena, so piezoelectric constants represented by *"i j"* indices such as d_{ij},in which *i* represent the direction of polarization or electrical input/output and j represents the direction of strain or mechanical input/output. The subscripts are defined in Cartesian coordinate system including X Y & Z (Fig.1.3). Numbers 1- 3 assign to longitudinal parameters and $4 - 6$ represent the shear mode.

Fig 1.3*Directions in a piezoelectric unit cell according to Cartesian system*

$$\mathbf{d}_{ij} = \frac{dx}{dE}$$

Unit of Piezoelectric strain constant (d) is m/V

d_{ij} is the coefficient resulted due to polarization in *i* direction by applying the mechanical force in *j*direction

(ii) Piezoelectric voltage constant (g):

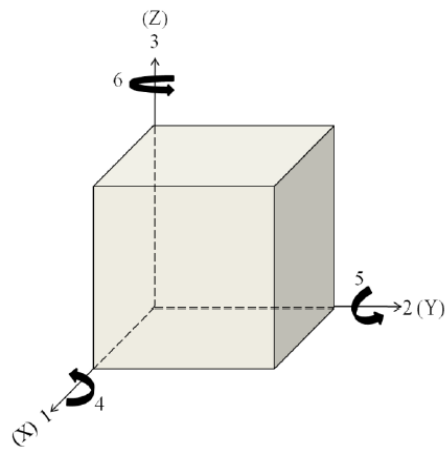The tensor that defines the generation of electric field (E) on application of stress (X) is known as piezoelectric voltage constant.

$$\mathbf{g}_{ij} = \frac{dE}{dX}$$

Unit of g = nC/N

(iii) Electro mechanical coupling factor (k):

It is a factor that relates the coupling efficiency between electrical and mechanical energy. It defined as-

$$k^2 = \frac{StoredMechanicalEnergy}{storedElectricalEnergy}$$

1.4 Piezoelectric Materials:

The first known piezoelectric material is quartz. But piezoelectric materials are numerous, the most used are: Quartz (SiO_2), Gallium orthophosphate ($GaPO_4$), Lithium Niobate, Barium titanate, piezo polymers (PVDF, Polystyrene, Polypropylene). Among all known materials lead based ceramics are most important and show high piezoelectricity.

1.4.1 Lead based piezoelectric materials:

- **Lead Zirconate Titanate ($Pb(Zr,Ti)O_3$):**

Lead Zirconate Titanate (PZT) is the solid solution of the $PbZrO_3$ and $PbTiO_3$. The solution $Pb(Zr_{1-x} Ti_x)O_3$ exhibits interesting piezoelectric and ferroelectric properties. It has the perovskite structure with Zrand Ti randomly arranged in the B site of the perovskite. By

varying the composition (value of x),the properties change with phase transformations as shown in the phase diagram of PZT[4].Fig.4.1
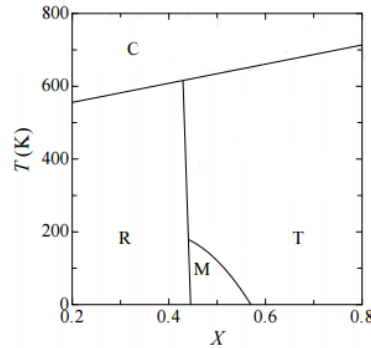

Fig.1.4. *Phase diagram of PbZrO₃ – PbTiO₃[4]*

The titanium rich region is tetragonal and undergoes a phase change from tetragonal to cubic on increasing the temperature. The zirconium rich rhombohedral region contains two symmetries, including low temperature form with R3c symmetry and a high temperature form with R3m symmetry. PZT with x ~ 0.5 crystallizes in the unique region of the phase diagram called the morphotropic Phase Boundary (MPB), in this region both phases (rhombohedral and tetragonal) can coexist. In the vicinity of the MPB region PZT shows high piezoelectric properties. (Where d_{33} = 600pC/N)[5]. In the MPB region the presence of more number of active polarization orientations decreases the energy barriers for switching the spontaneous polarization vector. Because of low energy barrier for switching of polarization PZT shows high piezoelectric properties in the vicinity of the MPB region. Fig.5 shows the active polarization orientation in the tetragonal and rhombohedral phases.
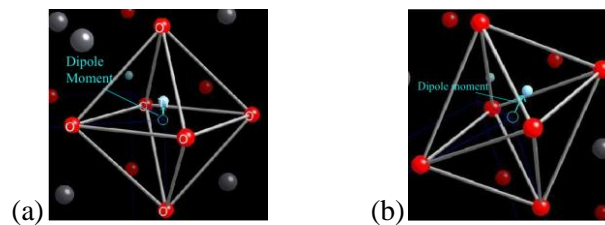

Fig1.5 *(a)Tetragonal phase: Ti motion in O octahedral is in [100] direction, dipole moment generates in [100] direction so total possible dipole orientation are 6. (b) Rhombohedral phase: the movement of Ti atom is symmetrical along [111] direction, dipole generates in [111] direction, it gives it 8 possible dipole moment directions. [3]*

5

Other lead based piezoelectric materials become interesting to researchers after the discovery of PZT. So many complex compositions have been investigated intensively, some of them showed very interesting properties as well. Compounds like Lead Scandium Niobate(PSN), PMN-PT, PFN, PNN-PTetc. are the well known lead based piezoelectric materials, which are in great use for sensors, transducers and actuator applications.

Environment issues: Lead is one of the toxic known materials, and continuous exposure to this element causes serious damage to the human organs like kidney, heart and brain. Considering the toxicity of lead and its compounds, there is a general awareness for the development of environmental friendly lead-free materials as evidenced from the legislation passed by the European Union in this effect. [1] Several classes of materials are now being considered as potentially attractive alternatives to PZTs for specific applications.

1.4.2 Lead free piezoelectric materials:

There has been growing interest in developing the lead free piezoelectric materials that can replace the lead based piezoelectric materials. Intensive research has been done on related studies all around the world. Scientists have been working on bulk as well as thin films of lead free piezoelectric materials. One of the lead free piezoelectric materials which gained a lot of interest in last decades is – $BaTiO_3$(BTO) Barium Titanate is the most widely explored lead free ferroelectric material as it possesses good dielectric and piezoelectric properties in bulk as well as in thin films. $BaTiO_3$ substituted with small atom percentsofCa and Zrin A and B- sites respectively exhibit improved piezoelectric propertiesthatare comparable to the PZT. BTOsubstituted with Ca and Zr have been studied extensively in bulk after the research work of Wenfeng Liu and XiaobingRen in 2009[6]. But theBCZT(xBCT – (1-x)BZT) thin films are not studied extensively. Behavior of BCZT and its properties based on phase transitions in the vicinity of morphotropic phase boundary is explained specifically in chapter -2.

1.5 Motivation and objective:

A piezoelectric thin film is one of the key materials for miniaturizing electronic components. In micro electromechanical system (MEMS) applications, piezoelectric thin films can be applied in many kinds of electronic devices, such as actuators, resonators, and filters. In the recent years as the technology become the integral part for the human life so the usage of the electronic devises has been increased abruptly. But as the piezoelectric thin film market is dominated by the lead based piezoelectric materials which are hazardous to the health. After the RoHS (Restrictions on the use of certain Hazardous Substances) act by European community in 2006 [1], and after the research of BCZT in 2009, lot of investigations has been done on BCZT bulk ceramics. But the BCZT is not been explored that much in thin films except some of the efforts has been made [7]. This project is an effort to deposit the epitaxial thin films of BCZT (0.5BCT – 0.5BZT) on single crystalline Strontium Titanate ($SrTiO_3$) substrates. The main objectives of this project involve:

- Synthesis of BCZT ceramic by the solid state reaction route
- Substrate surface studies: Substrate plays a crucial role on growth of epitaxial thin films. Hence preparing a surface of a substrate by etching and annealing is mandatory. In this study the STO (001) substrates were chosen and utilized for further studies.
- Deposition of BCZT by the Pulsed Laser Deposition(PLD) method on the STO(001) substrate
- Morphology analysis of the BCZT film using AFM (Atomic Force Microscope) and SEM(Scanning electron Microscope)
- Structural analysis of the BCZT thin films with HRXRD(High Resolution X-ray Diffraction): It includes phase identification, epitaxial analysis, mosaic structure analysis and reciprocal space mapping of the thin film.

Chapter 2

Literature review

The continuous drive for miniaturization of devices demands fabrication of various materials in thin film form. Though there exists no strict definition for thin film, in the electronic industry a thin film device can range from few nm to micrometer thicknesses. Thin films possess very special and different properties from the bulk. We are using thin films in almost every area from electronic industries to defense sector. Wide range of their application includes the protection of a material from corrosion and oxidation, and also in filters, sensors, high temperature superconductor devises and memory devices. Properties of these thin films widely depend on the fabrication method.

Among the broad classification of methods of fabrication of thin films physical vapour deposition (PVD) is mostly utilized for fabrication of electronic materials due to the high purity achieved in such techniques. In PVD, the conditions at which the growth takes place play a crucial role like substrate temperature, pressure in deposition chamber. Substrate surface plays a crucial role in deciding the structure of the film. Thin films could be either amorphous, polycrystalline, textured and epitaxial in nature. Epitaxial films are most preferred for electronic device applications due to the superior property achieved through epitaxial thin films. In the case of epitaxial growth, selection of substrate for the deposition of thin film depends on the structure of the material which is to be deposited. In order to achieve, epitaxial thin films, lattice mismatch between substrate and film should be less than 5% [8]. In this project we used strontium titanate (STO) substrate which has a cubic crystal structure and the material of our interest BCZT (0.5BCT – 0.5BZT) films can be grown on it possessing a pseudocubic epitaxial relation.

2.1 Strontium Titanate ($SrTiO_3$ - STO):

STO has attracted special attention as a substrate for growth of complex oxides because of its chemical stability and small lattice mismatch with most other oxides ($SrRuO_3$, TiO_2 etc.). It is know that to achieve an epitaxial oxide thin film we need to provide single crystalline and atomically flat substrate surface. In the case of STO (001) the atomic layer stacking could be understood as two layers arranged alternatively, i.e. SrOand TiO_2.It is known from previous studies that the TiO_2 terminated surfaces provide higher stability as compared to

SrO terminated surfaces. Hence, in this work TiO_2 terminated $SrTiO_3(001)$ substrates were used. Procedure to obtain a TiO_2 terminated STO surfaces was first studied by *Kawasaki et.al.* in 1999[9], since then various techniques has been followed based on selective etching like using HCNO (Fulmic acid)[10] and DI water. Lots of research has been done on this STO(001) in order to achieve atomically flat surface. Heat treatment studies on STO(001) surface suggests the formation of some strontium rich non- perovskite such as Ruddelsden - Popper phase($SrO(SrTiO_3)$) [11].

SrTiO_3 possess cubic crystal structure with a lattice constant of 0.3905nm at room temperature. STO (100) crystal structure consists of alternative layers of charge neutral SrO and TiO_2 layers. The STO (001) surface can be prepared such that it has a SrO, TiO_2 or mixed termination. But the STO (001) crystal structure is known to have stable TiO_2 termination [12]. TiO_2 terminated STO (001) surface consists steps of height equal to inter planer spacing of (100) plane. In this work we tried to create TiO_2-terminated $SrTiO_3$ substrates because this substrate surface is in general regarded as stable and atomically smooth. It is often used as a substrate for complex oxides since it is chemically stable and has a small lattice mismatch with other oxides such as $SrRuO_3$, $LaNiO_3$ and TiO_2 . In this project we studied the etching and annealing effects on STO (001) in order to get TiO_2 terminated surface.

2.2. Barium Titanate (BaTiO₃):

Barium Titanate is one of the most widely explored lead free piezoelectric. It is having the perovskite structure as shown in Fig.1.2 (a), with Ti^{+4}ion in oxygen octahedra. The piezoelectric properties of $BaTiO_3$ depend on the rattling of Ti ion in the oxygen octahedra. $BaTiO_3$ possess good piezoelectric and dielectric properties and also it shows spontaneous polarization below the Curie temperature. According to the phase diagram of $BaTiO_3$ by A.VonHippel in 1950 [13], $BaTiO_3$undergoes many transitions from low temperature to high temperature. Above 393K, barium titanate has a cubic structure. This means it is Centro-symmetric and possesses no spontaneous dipole. With no dipole the material behaves like a simple dielectric, giving a linear polarisation. The Curie temperature (T_c) for $BaTiO_3$ is 393K. Below 393K, it changes to a tetragonal phase, with an accompanying movement of the atoms. The movement of Ti atoms inside the O_6 octahedra may be considered to be significantly responsible for the dipole moment [14].on further cooling at 285K structure changes from tetragonal to orthorhombic phase, which also possess spontaneous polarization. At 199K orthorhombic phase of $BaTiO_3$ changes to ferroelectric

rhombohedral phase. Figure 2.1 shows polarization vs temperature diagram of BaTiO$_3$. Before melting at 1891K, perovskite structure of BaTiO$_3$ dramatically converts in to hexagonal structure.
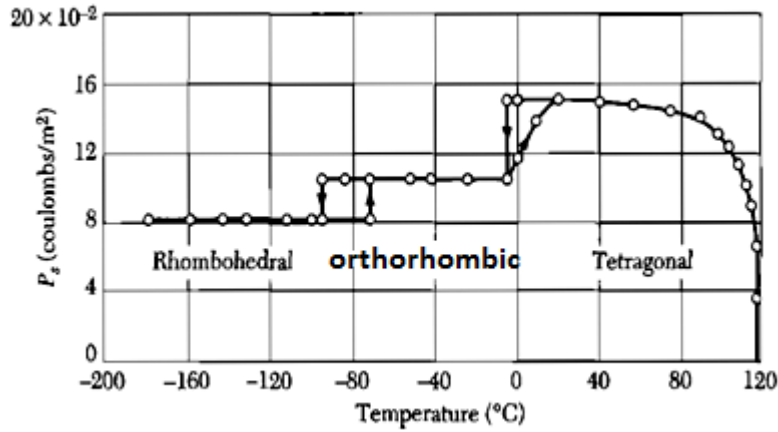

Fig2.1 *Polarization vs temperature curve showing the phase transitions in BaTiO$_3$* **[15]**

Several studies have shown that doping is one of the best known method to improve the material performance of electro ceramics. BaTiO$_3$ doped with Ca and Zr shows high dielectric permittivity, enhanced temperature stability and improved reliability compared to pure BaTiO$_3$. In next section the effect of Ca and Zr on the BaTiO$_3$ will be discussed respectively.

2.2.1   Effect of Ca on BaTiO$_3$:

The Ca^{+2} ion can be doped in BaTiO$_3$ by substitution solid solution where it replaces some of the Ba^{+2} ions from their sites and form (BaCa)TiO$_3$. The Ca^{+2} ion (ionic radius = 1.34Å) is smaller than the Ba^{+2} ion (ionic radius = 1.61Å) so by increasing the amount of CaTiO$_3$ in the BaTiO$_3$,unit cell volume will decrease. The phase equilibrium of BaTiO$_3$ − CaTiO$_3$ has been investigated by quenching, thermal analysis, and pellet melting methods**.** The temperature of the tetragonal-cubic BaTiO$_3$ inversion is lowered gradually to 378K by additions of CaTiO$_3$.The nature of the phase transition in a mixed system depends on the procedure adopted for the synthesis of the ceramics. Ceramics obtained by a semi wet route involving calcination of a mixture of Ba$_{1-x}$Ca$_x$CO$_3$ precursors with TiO$_2$ exhibit diffuse

ferroelectric phase transition. The diffusiveness in the phase transition increases with increasing Ca content within its solubility limit. The same ceramics, when prepared using the conventional dry route involving calcination of $BaCO_3$, $CaCO_3$ and TiO_2 particulate mixture, exhibit the usual $BaTiO_3$-type sharp transition. The difference in the nature of ferroelectric transition in the above-mentioned ceramics, when prepared by different methods, could be due to departure from this ideal situation and because of varying site occupancies of Ca^{2+} in them [16].

In $Ba_{1-x}Ca_xTiO_3$ piezoelectric coefficient has been improved from 180 to $360pCN^{-1}$ [17].The Curie temperature is increased to 136°C by adding the Ca^{2+} ions upto $x = 0.08$ and then reduced for higher contents [18]

2.2.2 Effect of Zr on BaTiO$_3$:

The Zr^{4+} ion mixes in the $BaTiO_3$ structure via a substitution solid solution, where it is placed in the Ti^{4+} site and forms barium zirconate titanate (Ba(Ti,Zr)O3). The Zr^{4+} ion (ionic radius = 87 pm) is larger and chemically more stable than the Ti^{+4} ion (ionic radius = 68 pm), and thus replacement of Ti^{+4} by Zr^{+4} suppresses the conduction developed by the electronic hopping between Ti^{+4} and Ti^{+3}, and leads to an enhanced dielectric constant and reduced leakage current in the $BaTiO_3$ structure. The piezoelectric and electrical properties in the $Ba(Ti_{1-x}Zr_x)O_3$ system have been investigated for different Zr concentrations, and it has been demonstrated that for compositions $0 \leq x \leq 0.1$ the ceramics show normal ferroelectric behavior, however, for compositions $0.10 \leq x \leq 0.42$ relaxor properties are indicated. It has been demonstrated that using a Zr/Ti ratio of 20/80 in the $Ba(Ti,Zr)O_3$ ceramics creates good piezoelectric and electrical properties in this system [19].

Recently, the lead-free $(1-x)Ba(Zr_{0.20}Ti_{0.80})O_3 - x (Ba_{0.70}Ca_{0.30})TiO_3$ system has been shown to possess a very high piezoelectric response. For x = 0.5 the d_{33} value was found to be 620 [6], it is more than the d_{33} value of the best known piezoelectric (PZT). The high piezoelectric response of this compound attracts researchers in the past decade. Lot of research has been done in order to understand the high piezoelectric response at a morphotropic phase composition (x = 0.5). In the next section the properties and phase diagram of this compound has been explained.

11

2.2.3   Barium Calcium Zirconate Titanate (BCZT):

After study the effect of the addition of the Ca and Zr in BaTiO$_3$ separately this section deals with the addition of Ca and Zr together in BTO. The basic approach to increase the piezoelectricity is to place the composition of the material in the proximity of the composition induced phase transition between two ferroelectric phases, like in PZT (explained in chapter 1). In 2009 Wenfeng Liu and Xiaobing Ren[6] used the same concept to increase the piezoelectricity in BCZT system, they kept the compositions of BCT and BZT near the pseudo morphotropic phase boundary and achieved good piezoelectric response with d$_{33}$ = 620pCN^{-1}. It was demonstrated that there was a tricritical point (TCP) in the phase diagram at x = 0.35 and T = 57 °C. At that point, the cubic-paraelectric, ferroelectric rhombohedral, and tetragonal phases meet each other. In the vicinity of the tricritical point, the polarization anisotropy vanishes, so that the dielectric permittivity and piezoelectric coefficient experience very strong enhancement. This result attracted the interest of researchers in this compound. Later in 2013 further investigation of the phase diagram revealed the presence of an orthorhombic phase of BCZT [20]. The updated diagram is shown in the Fig.2.2. For the composition at x= 0.32 to 0.9 the compound follow the phase sequence rhombohedral(R) – orthorhombic(O) – tetragonal(T) – cubic(C) from low to high temperature. This is identical to the parent BaTiO$_3$ phase sequence.
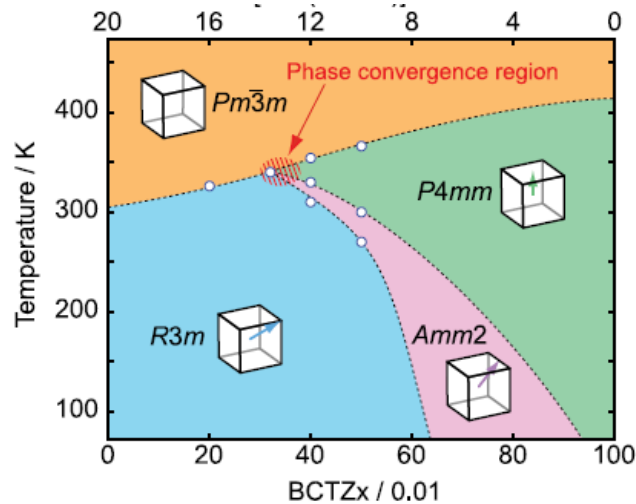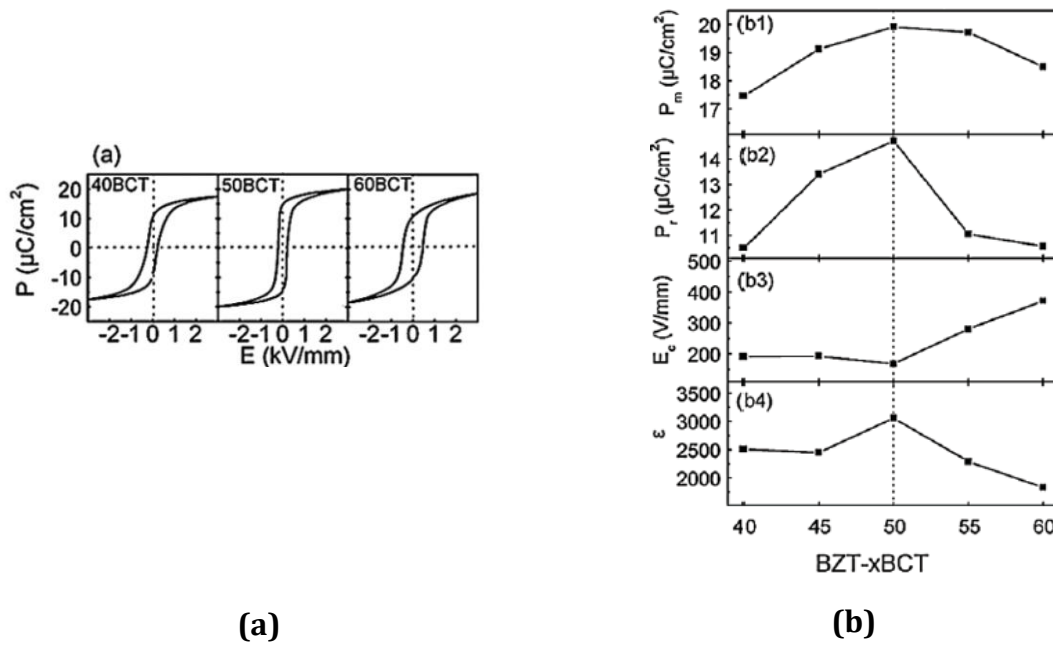

Fig 2.3 *Phase diagram of BCZT [20]*

Fig.2.3 *Various dielectric studies of xBCT- (1-x)BZT system by variation of the value of x (a) Hysteresis loops of 40BCT, 50BCT,and 60BCT.(b1) Saturation polarization, Pm, (b2) remnant polarization, Pr, (b3) coercive field, Ec, (b4) permittivity, [6]*

Piezoelectric properties: at x=0.5 the (x)BCT–(1-x)BZT system shows highest piezoelectric properties. Fig 2.3(a) shows the hysteresis curve of BCZT. The remnant polarization is $8\mu C/cm^2$, coercive field 168V/mm, d_{33} = 620 pC/N and dielectric permittivity is 3060 at x= 0.5. Fig 2.3 (b) shows that piezoelectric properties of this BCZT system are maximum for x= 0.5.

In summary, high piezoelectricity can be achieved in (x)BCT–(1-x)BZT system at composition in the vicinity of the morphotropic phase boundary. At this composition polarization anisotropy vanishes, which causes a very low energy barrier for polarization rotation and lattice distortion. High piezoelectricity and absence of lead in the compound makes it a potential candidate for replacement of PZT in future. This project is an approach to explore BCZT system in thin films. Next chapter deals with the experimental work carried out for the deposition of BCZT thin films and various characterization techniques used.

Chapter 3

Experimental

The experimental work carried out in this project includes the substrate treatment carried out in STO prior to deposition, actual deposition of BCZT (0.5BCT – 0.5BZT) thin films and the structural characterization of the same. As the substrate surface plays an important role in the quality of thin films it is important to study the surface treatment of the STO substrate. Hence, the substrate treatment of STO (001) was carried out.

3.1   Surface treatment of STO (001):

To obtain a stable substrate surface with smooth TiO_2-termination, a preparation treatment can be used in which selective chemical etching is used to remove the SrO surface plane. The total preparation procedure consists of:

- **Hydrolyzing as received sample**: ultrasonication by soaking an as-received substrate in DI water.
- **Etching**: Dipping the substrates in a BHF solution for 30 – 120 seconds to etch the SrO.
- **Annealing**: heat treatment of the etched substrates at 950-1000°C in oxygen ambience.

In this project we followed all the above mentioned steps by varying the parameters like etching time, annealing temperature etc.

3.2   Fabrication of BCZT thin films:

As we know that the conditions during the deposition decide the properties of the thin film fabricated, BCZT thin film were fabricated under various conditions. As BCZT is a complex material having a perovskite structure with Ba and Ca at the A-site, Ti and Zr on the B-site, pulsed laser ablation technique was chosen for the deposition of thin films of BCZT. PLD is commonly utilizedto deposit complex materials with maintaining the stoichiometry, (as mentioned in Chapter-2).

Few factors that are crucial in deposition of thin films are (i) substrate on which the deposition will take place, (ii) The target material which is going to be deposited and (iii) deposition conditions. The depositions were carried out in a high vacuum chamber with a base pressure of 2×10^{-6} Torr (Excel instruments). A pulsed KrF excimer laser firing at 248 nm and a possible energy range of 100mJ to 500mJ was utilized for the deposition.

3.2.1 Preparation of Target materials for PLD:

A dense target of BCZT was made by the solid state reaction route. Chemicals used were $BaCO_3$, $CaCO_3$, ZrO_2 and TiO_2. The reaction involved in the process is –

$$0.85BaCO_3 + 0.15CaCO_3 + 0.10\ ZrO_2 + 0.90\ TiO_2 \longrightarrow Ba_{0.85}\ Ca_{0.15}\ Ti_{0.9}\ Zr_{0.1}\ O_3 + CO_2 \uparrow$$

Steps involved:

1. All the chemicals were ground well in their stoichiometry ratios using agate motor. After mixing them for 1 hr, the fine powder was kept in muffle furnace for calcination.

2. Calcination: Calcination of the fine powder was done at 1200°C for 6 hrs. The heating and cooling rate were maintained at 5°C per minute.

3. Ball milling and pellet making: After calcinations powder was ball milled at 400rpm for 6 hrs. The fine powder was then pressed into the shape of a pellet of 20mm diameter and 3.5mm thickness after adding few drops of binder PVA (Poly Vinyl Alcohol). Total pressure used was 20KN for 60sec.

4. Sintering: For densification of pellet sintering was done at 1550°C for 5hrs.Heating rate was maintained at 3°C per minute upto 300°C , at 300°C further heating was stopped for completely removal of the binder. From 300°C to 1550°C the heating rate was 5°C per minute. Holding at 1550°C for 6 hrs results in densification of the pellet. After that a slow cooling rate of 3°C per minute was maintained.

3.2.2 Deposition of BCZT on STO (001) substrate:

BCZT films were deposited on the STO(001) substrate by Pulsed Laser Deposition technique.

(i)   Pulsed Laser deposition:

A schematic view of a typical PLD setup is given in Fig 3.1. In this schematic drawing the vacuum chamber and optics are depicted. Furthermore the target, heater with a substrate, plasma plumes and laser beam are shown. Typically a pulsed laser beam is focused on a rotating target, at an angle of 45º with respect to the target normal. During laser-target interaction electromagnetic energy is rapidly converted into thermal energy and creates a local melting on the surface of the bulk target material. Furthermore, the backward thrust experienced by the melt results in a forward ejection of the species called as plume which contains ablated species like atoms, particles and clusters. The plume expands towards the substrate surface and gets deposited. Continuation of the phenomenon results into growth of uniform thin film on the substrate of our choice. The period between two consecutive deposition pulses can be as long as many seconds. In this period ad-atoms and clusters can rearrange themselves on the surface when they overcome the energy barriers.
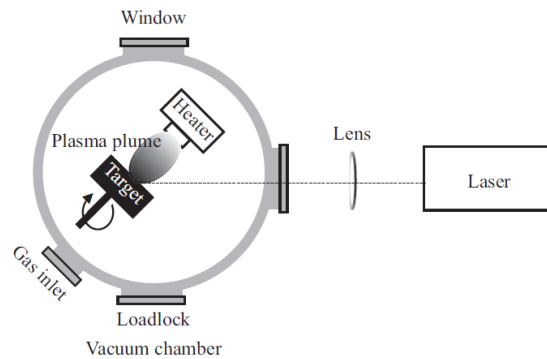

Fig.3.1 *Schematic of the Pulsed Laser Deposition (PLD)*

Though PLD has the capability to produce stoichiometric multi-component films, the uniformity is restricted to smaller area and hence, this technique is limited to laboratory investigations only. Some of the important steps in PLD are – interaction of laser with

material, plume formation, nucleation and growth on the substrate. Factors which affect the quality of film and also the structure of the film are as follows-

- Laser energy: A pulsed laser is focused onto a target of the material to be deposited. For sufficiently high laser energy density, each laser pulse vaporizes or ablates a small amount of the material creating a plume. The ablation depends on the energy of laser beam.

- Pressure in the vacuum chamber: The spatial distribution of the plume is dependent on the background pressure inside the PLD chamber. Also the time of flight of the ablated atoms depends on the oxygen pressure inside the chamber.

- Substrate temperature: For the adsorption of the ablated atoms/ions the substrate temperature plays an important role. Substrate temperature decides the ad-atom mobility which effectively decides the residence time and sticking coefficient of the adsorbed atoms on the substrate surface.

- Cooling rate: The quality of the film depends on cooling rate of the substrate after deposition.

(ii)   Epitaxial thin films:

Epitaxy means growth of a material on a substrate layer by layer with a crystallographic relation with the substrate. The presence of the crystallographic relation with substrate reduces the density of interfacial defects, which is crucial for the end application of electronic materials. Epitaxial thin films can be divided into two types (i) hetero-epitaxy (film and substrate are different materials) and (ii) homo-epitaxy (film and substrate are same materials). In hetero-epitaxy unmatched lattice parameters of substrate and film causes strained or relaxed growth and can cause interfacial defects. Such deviations from normal would lead to changes in the electronic, optic, thermal and mechanical properties of the films. A pseudomorphic layer is the one which have the same lattice parameters as of substrate. In order to grow pseudomorphic layer the lattice mismatch between substrate and film should not be more than 9%, apart from lattice mismatch layer thickness also may affect the pseudomorphic layer. Beyond a critical thickness strain energy is released and gives rise to misfit dislocations at the interface.

Substrate temperature is an important factor in deciding the epitaxial growth of thin film. As explained in Thornton diagram (Fig 3.2) if the ratio of substrate temperature to the melting temperature of the material is more than 0.8 then the recrystallized grain structure grows (epitaxy), if this ratio is less than 0.5 porous structure separated by voids form.
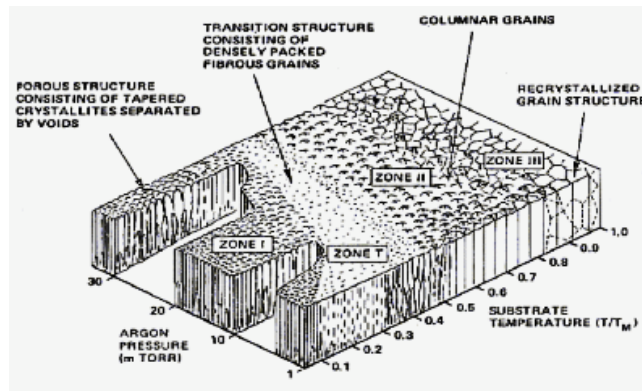
Fig 3.2 *Thornton diagram: Microstructural evolution of films as a function of generalized temperature ($T_{substrate}/T_m$) and pressure [21]*

3.3   Characterization Techniques:

Characterization techniques used in this chapter involves AFM (Atomic Force Microscopy), SEM (Scanning Electron Microscopy) and HRXRD (High Resolution X-ray Diffraction). Morphological studies have been carried out by AFM and SEM, while structural characterization of the deposited films has been studied by HRXRD. The fundamentals of each technique are explained below.

3.3.1   Scanning Electron Microscopy:

The scanning electron microscope (Carl Zeiss Supra 40) was used for obtaining high resolution micrographs BCZT thin films. The micrographs were used to study the morphology and the quality of the growth. Secondary electrons (result from interactions of the electron beam with atoms at or near the surface of the sample) facilitate the study of morphology and topography of samples.

3.3.2   Atomic Force Microscopy (AFM):

AFM(*Bruker instruments*) was used for obtaining morphology images of STO(001) substrates surface and BCZT thin films. Atomic Force Microscope (AFM) consists of anatomically sharp tip mounted or integrated on the end of a tiny cantilever spring which is moved by a mechanical scanner over the surface to be observed. Every variation of the surface height varies the force acting on the tip and therefore varies the bending of the cantilever. This bending is measured by an integrated stress sensor at the base of the cantilever spring and recorded line by line in the electronic memory. All the AFM images in this project have been taken in tapping mode.

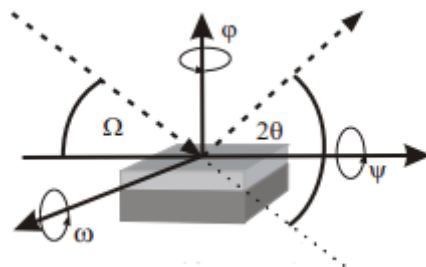### 3.3.3 HRXRD (High Resolution X-ray Diffraction)

Fig3.3 *Schematic of the goniometer angles of a HRXRay unit.*

HRXRD (Bruker instruments) was used for the structural characterization of the BCZT thin films. HRXRD works on the Braggs law, the sample rotation in all three axis as shown in Figure 3.3, makes it a very useful technique to characterize structure of thin films, thickness, roughness and also the strain in the films. Cu K-alpha x-rays (1.54Å) were used to collect the diffraction pattern of the BCZT thin films. Various modes of scans were used for obtaining different information from the samples. Θ-2Θ scan was performed to check the phase purity, rocking curve analysis was done to check the mosaic structure of thin film, reciprocal Space mapping(RSM) was carried out in order to calculate the strain, degree of relaxation and in-plane lattice parameter of the film.

Chapter 4

Results and Discussions

This chapter deals with the results and discussion of the experimental work performed in this project. The discussions in this chapter can be divided into two sub categories (i) substrate analysis, (ii) BCZT thin film analysis.

4.1   Substrate Studies: Before starting the surface treatment of STO(001) surface structural analysis and morphological analysis has been done on the pristine sample

4.1.1   Analysis of pristine sample:

4.1.1.1 Structural analysis of STO (001)

The diffraction pattern of the commercially purchased STO substrates was analyzed by HRXRD, to confirm the orientation of STO. Figure 4.1 shows the conventional theta- 2Θ scan with a monochromatic beam of Cu $K_{\alpha1}$(1.5401 Å).
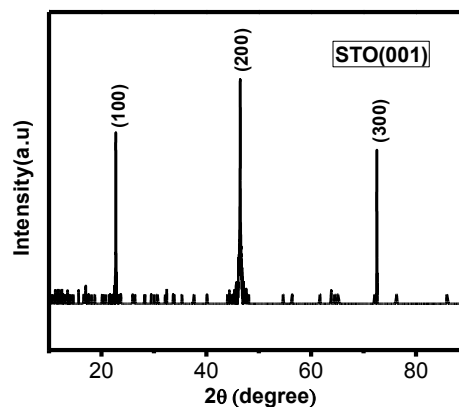

Fig. 4.1 *X-ray diffraction pattern of STO (001) substrate*

The obtained pattern in figure 4.1 confirms the single crystalline nature of the STO substrates with (001) orientation. The Bragg peak obtained at $2\Theta = 22.74°$ arises from the

(100) plane and their respective higher order reflections on higher angles was observed. The out of plane lattice parameter of STO (001) was calculated from the conventional Bragg relation and was found to be 3.905Å. The obtained value coincides well with the available ICDD data base no.18 - 1935 of STO.

4.1.1.2 Morphology of pristine STO (001):

The morphology of the as received pristine STO(001) is shown in the Fig.4.2. The scan was performed for the $25\mu m^2$ area in tapping mode. Surface of the substrate is found to possess relatively lower roughness. The average surface roughness was found to be 0.4 nm. Difference between the image's three-dimensional (figure 4.2 (b)) surface area and its two-dimensional, footprint area is found to be 0.205%, which shows that surface is very smooth
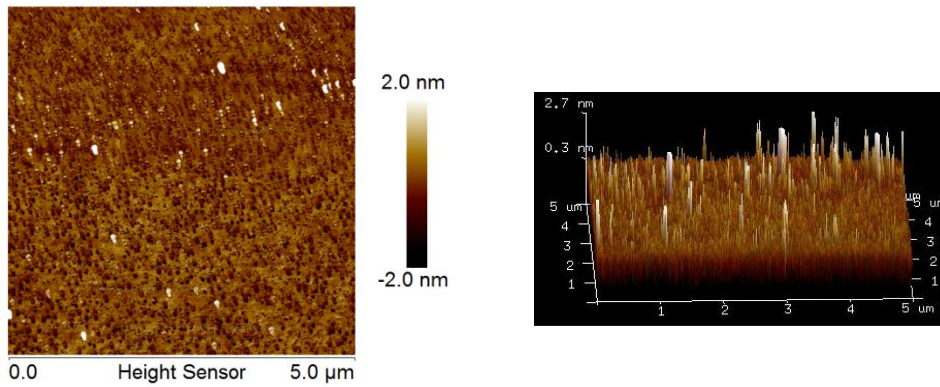

Fig.4.2 *AFM images of STO(001) substrates*

4.1.2 Substrate treatment

As explained earlier the substrate surface plays a crucial role in defining the performance of the electronic material. Hence, to obtain a smooth and specific termination on the STO substrates, certain procedure available in the literature were followed. [12]. It is known that such treatments would result in TiO_2 termination in STO (001) substrates. The details of the experiments are as follows:

1   Hydrolyzing as received sample:

In this procedure soaking the as-received substrate in deionized water is important to hydroxilize SrO, and $Sr(OH)_2$ formed on the surface as well as on edges of terrace island and hole, this $Sr(OH)_2$ dissolves faster in a buffered HF-solution (NH_4F : HF=7 : 1, pH=4.5)compared to TiO_2. Hence the formation of $Sr(OH)_2$is crucial in order to achieve TiO_2 terminated surface. The incomplete formation of $Sr(OH)_2$ might lead to islanding of strontium on the surfaces, which will increase the roughness and result in undesired termination.
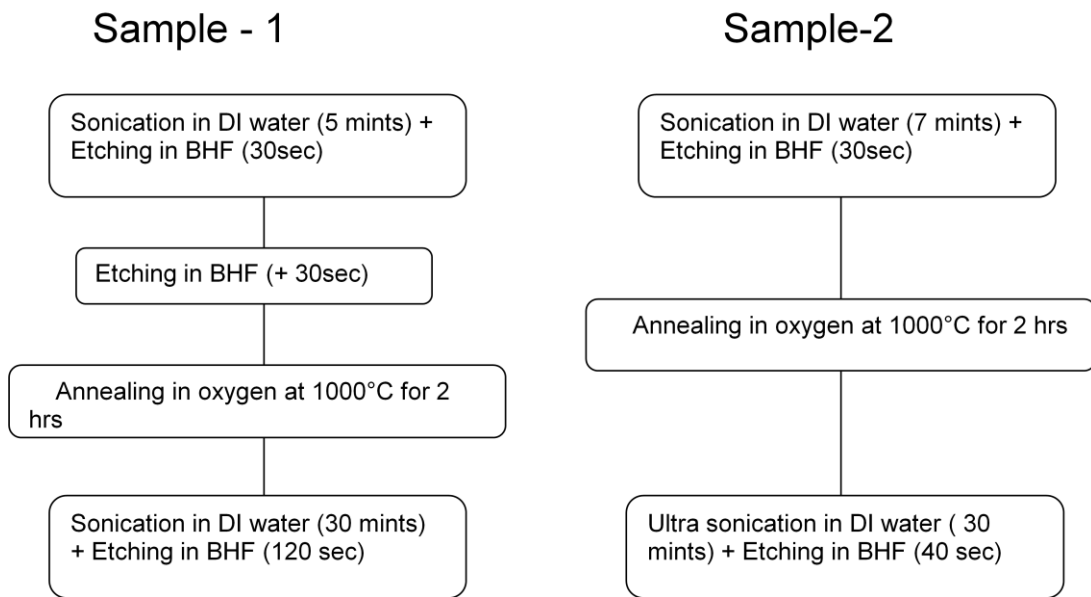
2   Etching:

In the second step, the $Sr(OH)_2$ formed in first step is etched using buffered HF solution (NH_4F : HF :: 7 : 1) of pH value 4.4 – 4.6,the pH value of solution plays very important role and it facilitates removal of basic $Sr(OH)_2$ and hence also called as selective etching. Solution with higher pH value creates some etch pits on the surface because of incomplete removal of strontium from the surface. During etching the SrO plane below the TiO_2 layer also etched sideways and also the holes and terraces on the surfaces. Etching time was also needed to be optimized, because less etching time may lead to incomplete removal of SrO, and long etching time may create etch pits on the surface. After etching; for complete removal of etchant from surface the substrates needs to be rinsed in DI water. On successful completion of etching TiO_2 terminated STO with atomic level steps of height d_{100} will be generated on the surface with minor oxygen defects. In order to reduce the surface defects and smoothen the surface annealing at elevated temperatures with oxygen ambience is mandatory.
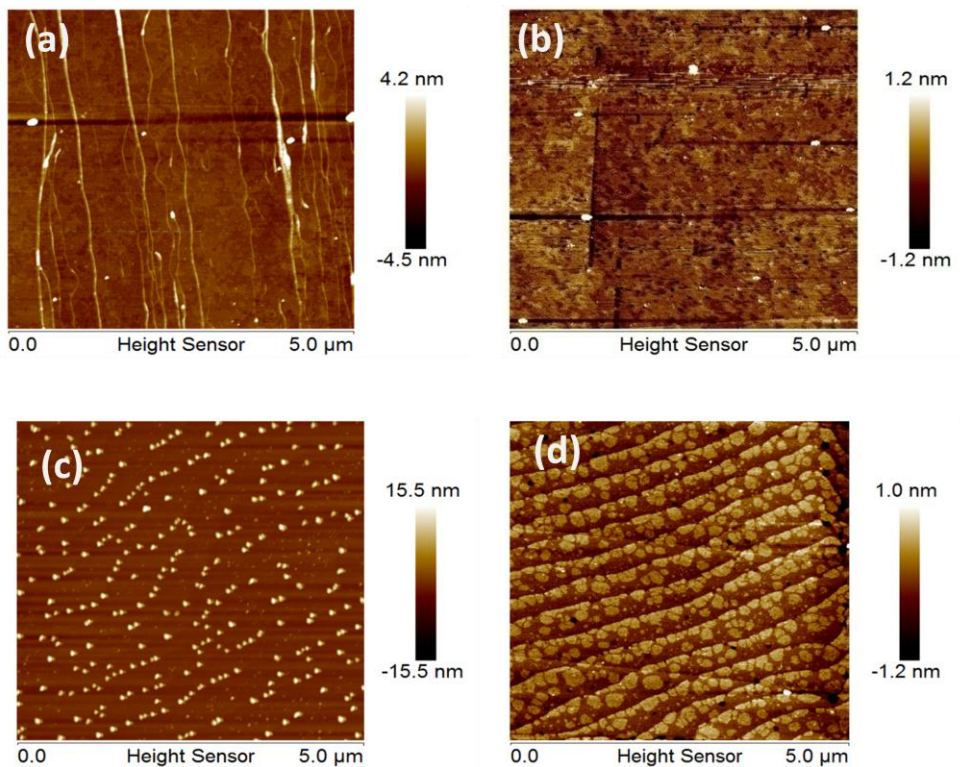
3.   Annealing:

Annealing of the etched substrate in oxygen environment leads to atomic reorganization on the surface. During annealing the diffusion process alters the step length and edges in order to minimize surface energies. The surfaces become atomically flat and exhibit clear step terrace structures with a sharp straight line at step edges having the theoretically expected single unit cell height.

Above mentioned step need to be followed in order to achieve the preferred surface on STO(001). In order to optimize the etching time and annealing time we performed various steps on two samples. After each step morphological studies were performed by AFM

Sample - 1

```
┌─────────────────────────────────┐
│ Sonication in DI water (5 mints) + │
│ Etching in BHF (30sec)            │
└─────────────────────────────────┘
              │
   ┌──────────────────────────┐
   │ Etching in BHF (+ 30sec)  │
   └──────────────────────────┘
              │
┌─────────────────────────────────┐
│ Annealing in oxygen at 1000°C for 2 │
│ hrs                               │
└─────────────────────────────────┘
              │
┌─────────────────────────────────┐
│ Sonication in DI water (30 mints) │
│ + Etching in BHF (120 sec)        │
└─────────────────────────────────┘
```

Sample-2

```
┌─────────────────────────────────┐
│ Sonication in DI water (7 mints) + │
│ Etching in BHF (30sec)            │
└─────────────────────────────────┘
              │
┌─────────────────────────────────┐
│ Annealing in oxygen at 1000°C for 2 hrs │
└─────────────────────────────────┘
              │
┌─────────────────────────────────┐
│ Ultra sonication in DI water ( 30 │
│ mints) + Etching in BHF (40 sec)  │
└─────────────────────────────────┘
```

Above shown flow chart is representing the various steps performed on the STO(100) by varying the etching time and annealing time. After each step morphological studies were carried.
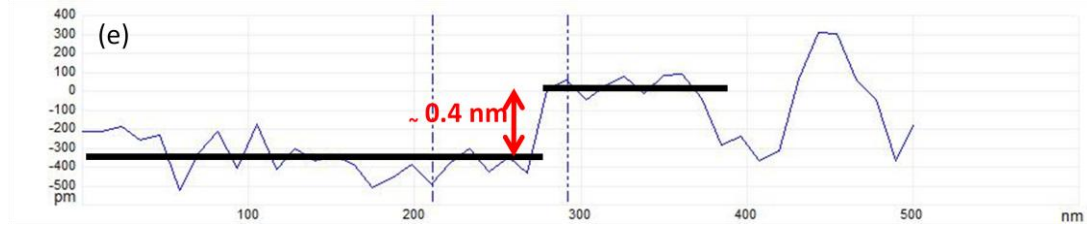
4.1.2.1 Sample 1:

Fig 4.3: *AFM images of sample-2 in tapping mode, (a) After 30sec etching ,(b) After 60sec etching, (c) After annealing at 1000°C for 2hrs, R = 2.46nm, (d)) After 30mins sonication and 120sec etching (e) Line profile across a step on the STO substrate revealing the step height (~ 400 pm)*

Figure 4.3 shows the AFM images obtained for sample 1, at various steps of processing. After 30sec etching the average roughness of the substrate increased from 0.4nm to 0.9nm. The increase in surface roughness is evident from the white streaks running across the image, which are vertically taller than the rest of the regions in the image. Such regions could have resulted from the incomplete removal of SrO and hence, we decided to increase the duration of the etching. On further etching the substrate for 30 seconds the morphology was improved and hence in total a 60 second etching for the given pH value was needed. Figure 4.3 (b) confirms the improvement in surface morphology on further etching process. After etching for 30 more seconds, the roughness of the sample decreased because of the enhanced removal of the strontium from the surface. Average roughness was found to decrease from 0.9 to 0.6nm.

Followed by the etching process, the substrate was annealed in the oxygen atmosphere at 1000°C for 2 hrs. a strange pattern of islands of average height 13nm were observed on the surface which was similar to the earlier observations of *K. Szot and W.Speir*. The studies on those islands with Auger electron microscopy had confirmed that those islands are mainly of SrO.[11] The restructuring of the surface region are expected to arise due to the redistribution of material and formation of non perovskite phases at elevated temperatures, like Sr-enriched phases called Ruddelesden-Popper and various forms of strontium oxide. Again to remove the Sr enriched area after annealing hydroxylation and etching in BHF was done for 32minutes. Steps formed on the surface but because of the less pH value of etchant some etch pits are formed on the surface. The average roughness was found to be 0.36 nm, which got reduced as compared to the pristine sample and most importantly it is close to the lattice spacing of STO, which is evident from the line profile across a step shown in figure 4.3 (e). Thus the surface treatment has resulted in the step formation in the STO due to the miscut present and the removal of SrO, however, from the observation of weak spots of

24

height contrast, we believe that those could be the remains of SrO left on the surface. Precise optimization of the pH might result into atomic flatness as expected in the STO substrates.
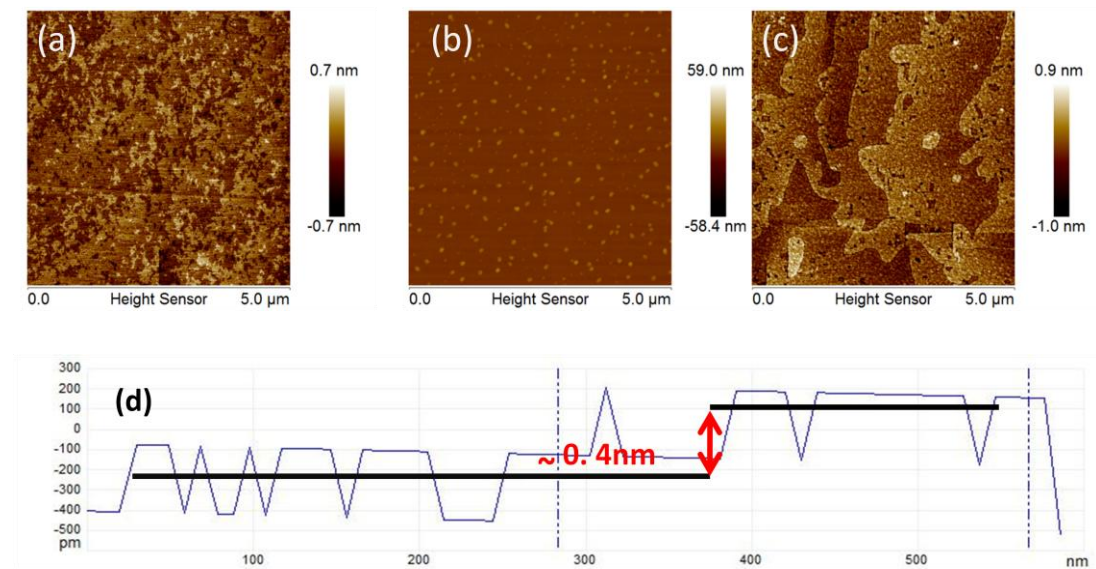
4.1.2.2 SAMPLE – 2

Fig 4.4: *AFM studies of Sample 2 (a) step 1: Surface morphology of STO after etching, (b) step 2: after annealing @ 1000°C for 2 hours, (c) step 3: etching for removal of SrO islands (d) Line profile of the surface steps observed in sample 2.*

In sample 2 Fig 4.4(a) shows AFM image after 7 minutes sonication followed by 30sec etching so we got very less roughness it shows that by increasing the sonication time surface quality has improved as compared to sample- 1. Fig 4.4(b) shows AFM image after annealing at 1000°C for 2 hours similar islands formed and it is clear that Sr is diffusing from the bulk to surface and suffers oxidation, Fig.4.4(c) after increasing the hydroxylation time in DI water and by increasing the etching time the atomic step like surface evolved with an average surface roughness close to 0.3 nm. Fig 4.4(d) shows the line profile taken from the surface of the STO substrate has a step like feature with step height varying between 0.3 to 0.5 nm at different regions of the sample. In summary a sequential processing of the STO substrates like, etching, annealing and further etching provides the required surface feature of the STO (001) substrates.

4.2   Characterization of BCZT:

4.2.1 Structural characterization of BCZT bulk and polycrystalline thin films

Phase pure BCZT powders were synthesized by solid state reaction route and dense ceramic pellets were utilized as target materials for laser ablation. Initially, polycrystalline films were deposited on platinum coated Si substrate, to study the phase formation temperature and to obtain knowledge on the quality of the films that were deposited. The polycrystalline films with varying temperature were deposited and were characterized by conventional X-ray diffraction to confirm the phase formation. Fig 4.5 shows the X-ray diffraction pattern of BCZT ceramic pellet and polycrystalline films grown at different substrate temperatures. Phase purity was observed in all the films deposited at 600, 650 and 700°C. The studies clearly revealed that the phase formation and purity of the same could be achieved at 600°C. In terms of quality of growth, the 700°C grown films exhibited a smoother and dense morphology, however, the defect densities were relatively larger and hence high leakage current was observed.
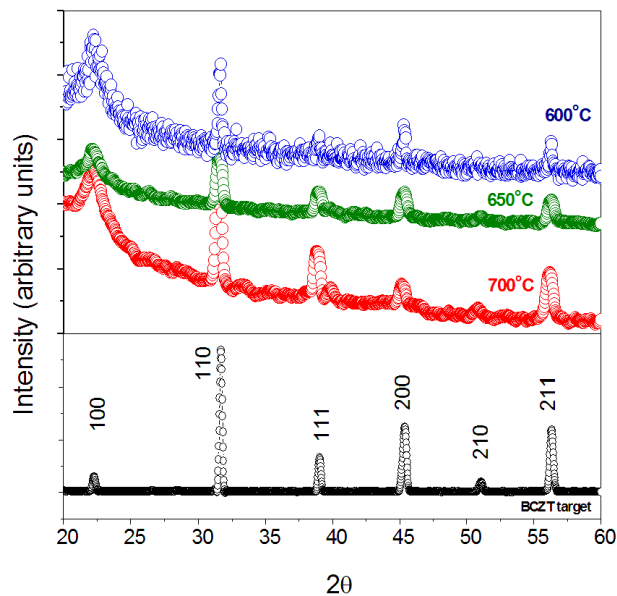

Fig. 4.5 X-ray *diffraction pattern of BCZT target and polycrystalline films at temperatures 600, 650 and 700°C [22]*

The preliminary studies on polycrystalline thin films clearly revealed that the optimum temperature would be between 600 and 675°C. Since, our major objective is to grow epitaxial thin films relatively larger temperatures are preferred, to facilitate the

26

recrystallization process [22] Thus, the parameters for deposition of epitaxial BCZT thin films on STO(001) substrates were carefully chosen. Given below table presents the various parameters used for the deposition of the different samples. For the analysis 3 samples were prepared at three different temperatures, with rest of the conditions remaining the same. The naming of the samples was done based on their deposition temperatures, like, i)**BCZT-600**(BCZT film deposited at 600°C), ii) **BCZT- 650**(BCZT film deposited at 650°C) and iii) **BCZT-675**(BCZT film deposited at 675°C)

Table 4.1 *Deposition parameters used for BCZT thin films*

Parameters	BCZT-600	BCZT-650	BCZT-675
Base pressure	8×10^{-6} Torr	8×10^{-6} Torr	8×10^{-6} Torr
Laser beam energy	250mJ	250mJ	250mJ
Laser repetition rate	5Hz	5Hz	5Hz
Oxygen pressure	100 mTorr	100 mTorr	100 mTorr
Deposition duration	6000 pulses	6000 pulses	6000 pulses
Substrate temperature	600° C	650° C	600° C

4.2.2 Surface Morphology of BCZT thin films on STO(001) substrate:

The morphology of the BCZT thin films on STO (001) was studied using an Atomic Force microscope operating under tapping mode. The scan was performed on each sample for the 100μm^2 area in tapping mode. Analysis of surface roughness and quality of film for each sample is discussed below.

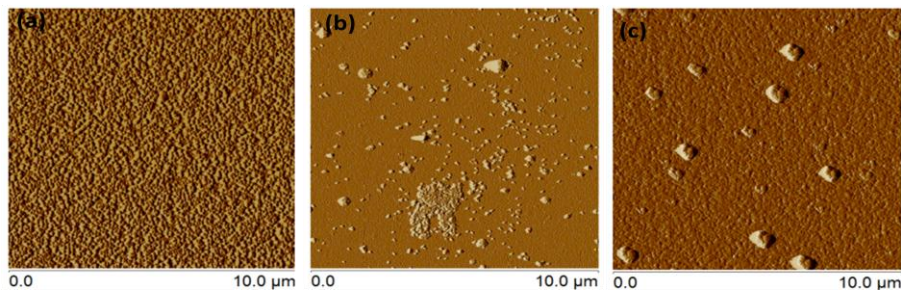**Fig 4.6***AFM images of (a) BCZT-600, (b)BCZT-650 and (c) BCZT- 675*

(i)   BCZT- 600

Fig 4.6(a) shows the surface morphology of the BCZT thin film deposited on STO(001) substrate at 600°C. The arithmetic average value of the surface roughness was found to be 16 to 17 nm. Difference between the 3D surface morphology and the 2D image was found to be 17%, which shows that the surface is rough with non-uniform growth. Though an island growth is observed, the orientation is believed to be dominated by the substrate orientation. Hence, those overgrown regions could be false nucleation sites with accelerated 3D growth and not grains and/or particulates with different orientation.

(ii)   BCZT -650

Fig 4.6(b) shows the surface morphology of the BCZT thin film deposited on STO(001) substrate at 650°C.In this case average roughness is found to be 4nm, the difference between the 3Dand its 2D, footprint area is found to be 1.80%, which shows that the film has a smoother morphology than the BCZT 600 sample. However, the sample is not completely free from overgrown nucleation sites.

(iii)   BCZT – 675

Fig 4.6(b) shows the surface morphology of the BCZT thin film deposited on STO(001) substrate at 675°C.In this case though the morphology was clearly dominated by overgrown nucleates, that effectively roughen the surface in comparison to BCZT 650.

In summary, the morphological studies using AFM revealed that BCZT thin films grown at 650°C possess a smoother morphology in comparison to the other temperatures, which was also evident from the microstructural studies performed using a scanning electron microscope.

4.2.3 Scanning Electron Microscope (SEM)

To further analyzing the surface morphology of BCZT thin films SEM images were recorded for all the samples. Figure 4.7 (a, b& c) shows the SEM images of all the BCZT thin films.
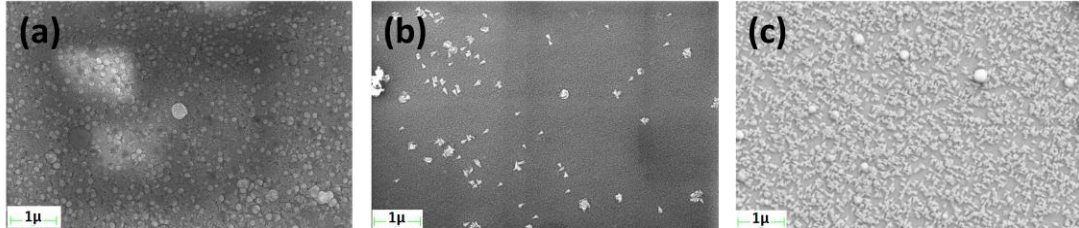

Fig 4.7 *SEM images of (a) BCZT-600, (b) BCZT – 650, (c) BCZT- 675*

(i)   BCZT – 600:

SEM image of the BCZT-600 is shown in Fig 4.7(a). Morphology of the sample is dominated by particles with a size distribution. Some over grown particles of size 200nm are visible and suggests that island growth on the substrate surface.

(ii)   BCZT-650

SEM micrograph of BCZT 650 shows uniform growth of thin film with some false nucleation on the surface. Some over grown particles of size equal to 50-70nm are also visible suggesting island growth at some regions. But overall BCZT – 650 possess a dense and narrow distribution of overgrown nucleates as seen in Fig.4.7 (b).

(iii)   BCZT - 675

SEM image of BCZT – 675 shown in figure 4.7 (c) clearly shows that on increasing the temperature, the density of false nucleates is enhanced and we could observed a larger number of overgrown nucleates with clear faceted feature. Though there is an enhancement in the overgrown nucleates over the surface, we believe they maintain the similar crystallographic orientation of that of the substrate and with the rest of the film.

The micro-structural analysis of the BCZT thin films supports the conclusions from the morphological studies done by AFM and in addition establishes the fact that the films grown at $600^{o}C$ possess particulates with spherical features. However, a film grown at 650 and 675 has a relatively smoother morphology and in addition they possess over grown nucleates with faceted features. This was further confirmed from the detailed structural analysis performed under HRXRD unit

4.2.4   X-ray Reflectivity studies (XRR):

The x-ray reflectivity studies were performed for all the samples (not shown) and it was evident that the surface morphology and the interfacial roughness of the samples were in the range of 30-40 nm, which corroborates well with the AFM and microstructural studies performed. However, the thicknesses of the films were relatively larger and was found to be in the range of 700-900nm.
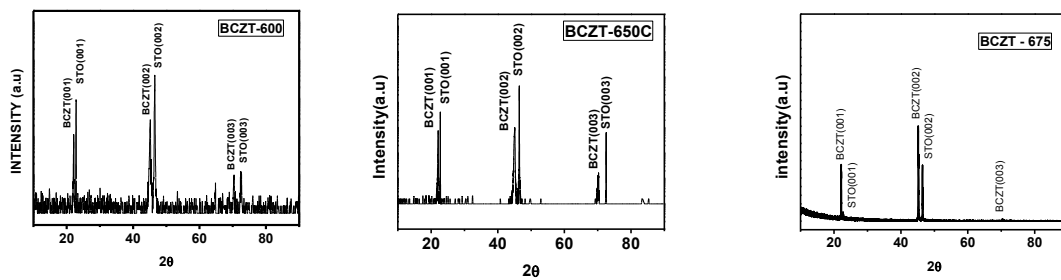
4.2.5   Θ - 2Θ scan:

Fig 4.8 *X-ray diffraction pattern of BCZT thin films(a)BCZT-600, (b)BCZT-650, (c)BCZT-675*

Figure 4.8 (a,b& c) shows the theta – two theta pattern recorded for the BCZT-600, BCZT-650 and BCZT-675 thin films. The pattern clearly reveals that the films were highly oriented along the <001> direction as of the substrate. Though the morphology studies revealed particulates and overgrown nucleates are present, none of the sample possessed grains of different orientation apart from the substrate. The peak positions were matched with the ICDD data base and found to be in accordance with the data [21].The out of plane lattice parameter ($d_{<001>}$) of BCZT-600 and BCZT-650 were found to be ~ 4.016(3)Å.The diffraction intensity of BCZT-675 thin film has a higher intensity of film than that of the substrate. This could be due to the large thickness (~1.2 μm), of the film. The larger thickness of the BCZT-675 is also evident from the x-ray reflectivity studies. The reflectance fringes obtained for BCZT-675 was found to have a periodicity half of that of 600 and 650°C grown films. It is interesting to note that the growth rate of these BCZT films are highly dependent on the growth temperature irrespective of firing the same number of laser pulses for all three samples.

4.2.6 Rocking Curve analysis

The previous discussions clearly establish that the films were highly oriented along the substrate orientation. However, the quality of texture is commonly analyzed using rocking curve analysis. This analysis helps us identify the misalignment present among the grains. The presence of such minor misalignment among the grains is termed as mosaicity. Figure 4.9 (a) shows the schematic of a mosaic structure. To confirm the mosaic structure present in thin films, rocking curve analysis was done on BCZT thin film samples. In the rocking curve analysis the detector of the sample is fixed at a given 2Θ angle corresponding to the out of plane orientation observed in the theta-two theta scan. On fixing the detector in the angle of our interest, the sample is given a tilt such that the ω angle. Generally the value of 2Θ is fixed at the peak position of highest intensity peak. In this section rocking curve analysis of all the BCZT thin films has been discussed in detail. Fig 4.10 shows rocking curves of BCZT thin film samples. In the case of epitaxial thin films it is known that peak width obtained from omega scan is expected to be in the range of 0.01 to 0.5. However, for epitaxial thin films the value is expected to be lower than 0.3
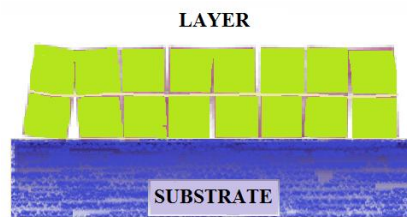

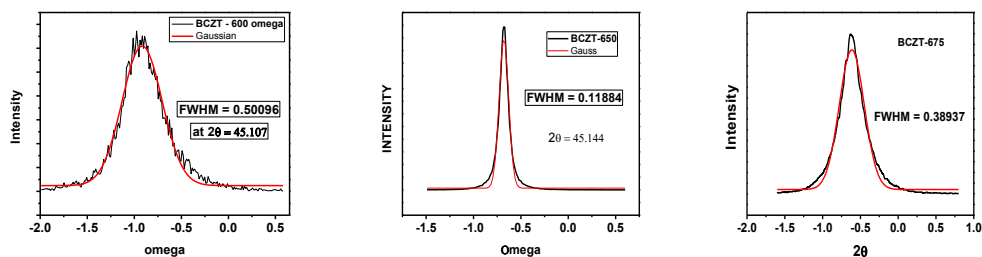
Fig.4.9(a) Mosaic structure example

Fig 4.10 Rocking curve analysis of (a) BCZT – 600, (b) BCZT – 650, (c) BCZT – 675

(i)   BCZT- 600

31

Rocking curve analysis of BCZT-600 (figure 4.10 (a)) was done by fixing the 2Θ value at 45.107°, because it is the highest intensity peak as confirmed from Θ - 2Θ scan. And along the omega (ω) axis the sample was tilted from -2° to 0.5°. The broadness in the peak shows the presence of mosaic structure or miss-alignment of the deposited grains. The FWHM was found to be 0.50 which shows the high misalignment present in the film grown at 600°C.

(ii)   BCZT – 650

Rocking curve analysis of the BCZT – 650 film was done by fixing detector at 2Θ = 45.144° (200). Sample was tilted along omega (ω) axis from -1.5° to 1°. Figure 4.10(b)

Shows the omega scan around (200) orientation of BCZT650 and the FWHM of the peak was found to be 0.1188° which indicates that there is very narrow misalignment among the grains present. As explained earlier, it is known that the smaller the omega scan width smaller the misalignment of grains in the thin films.

(iii)   BCZT-675

The rocking curve analysis of the BCZT – 675 is shown in figure 4.10(c) and the FWHM of the peak was found to be 0.3893.

In summary the omega scan analysis clearly reveals that the film grown at 650°C exhibit high alignment among the grains. It is also worth noting that the BCZT-650 films also exhibited a smoother morphology in comparison to the other films.

4.2.7   Reciprocal Space mapping:

In recent years reciprocal space mapping has been established as a powerful tool for the strain and in-plane analysis of epitaxial layers and hetero structures. It is known to be a non-destructive technique and also probes larger area of the sample facilitating measurement of precise values of strain and relaxation [23].

Figure4.11 shows a plane of the reciprocal lattice of a given unit cell. The plane of diffraction is defined by the incident and the diffracted X-ray beams which are chosen to lie in the plane determined by the two crystallographicaldirections, namely [001] and [100]. The two small half circles (Laue zones, radius: $1/\lambda$, λ being the X-ray wavelength) and the large one (radius: $2/\lambda$) indicate the limits of accessibility for diffractometric measurements in the Bragg (reflection) geometry.
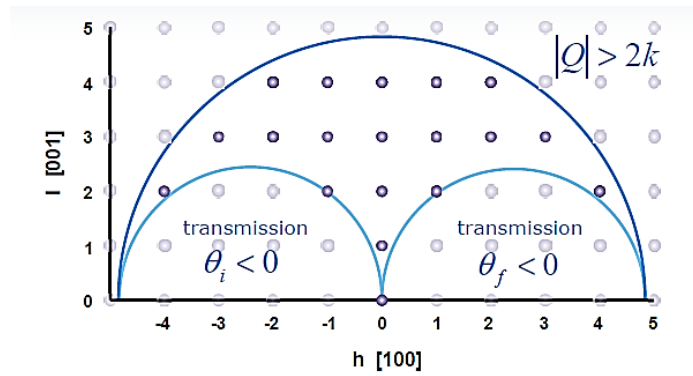
Fig.4.11 *Accessible region in reciprocal space for any given unit cell in Bragg geometry [24]*

From figure 4.11, one can decide the orientations suitable for the analysis for a given unit cell. The reciprocal lattice points in the vicinity of the Laue circle indicated with dark black arrow are the points that would yield high intensity and suitable for measurements. The reciprocal lattice points away from the Laue circle and closer to the circumference of the limiting circle are accessible points, but with weak intensity. Hence, the intelligent choice of choosing an orientation for study is crucial in performing reciprocal space mapping. Figure 4.12 details the various possible geometry in which, the analysis could be performed. ω is the angle between the incident beam and the sample surface, 2Θ is the angle between diffracted beam and the transmitted incident beam. It is know that when the diffraction vector becomes equal to the reciprocal lattice vector, the Bragg's condition is satisfied. Three type of scans are possible to obtain aRSM ,(i) rocking curve (by fixing 2Θ) (ii) Detector scan(by fixing ω) and (iii) $2\Theta/\omega$ or $\omega/2\Theta$ scan. The schematic representation of all three different scans is shown in figure.4.12
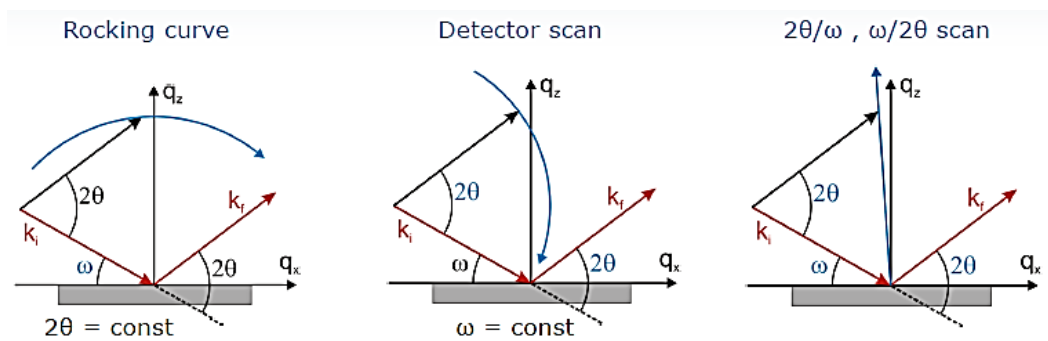

Fig.4.12 *Possible geometrical scans in RSM at a given instant of time [24]*

33

In this project we performed detector scan mode (figure 4.12: middle) on all the BCZT thin film samples and on STO (001) substrate to obtain the RSM images. The analysis could be performed in both symmetric (ψ=0, Θ=ω, refer figure 3.3) and asymmetric geometry ($\psi\neq$ 0, $\Theta\neq\omega$, refer figure 3.3). In symmetric geometry the scan was performed around(200) reciprocal lattice point and in asymmetric geometry the scan was performed around (103) reciprocal lattice point. Figure.4.13 shows the scanned area in both the cases, the red and green circle in the pictures represent the (200) and (103+) scanning area.
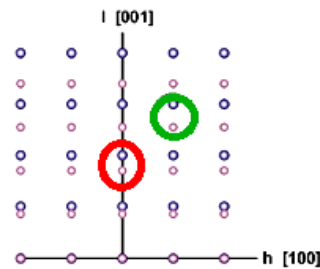

Fig.4.13 *Red circle represents (200) scan area in reciprocal space, green circle represents (103) scan area in reciprocal space*

Initially the RSM scans were performed on the STO(001) substrate that was treated similar to the deposition conditions, except for the deposition.

(i)   STO(001) substrate:

As explained earlier all the RSM scan was performed in the detector scanning mode and figure 4.14 shows the typical RSM image obtained for the STO (001) substrate that has been treated to mimic the deposition conditions.
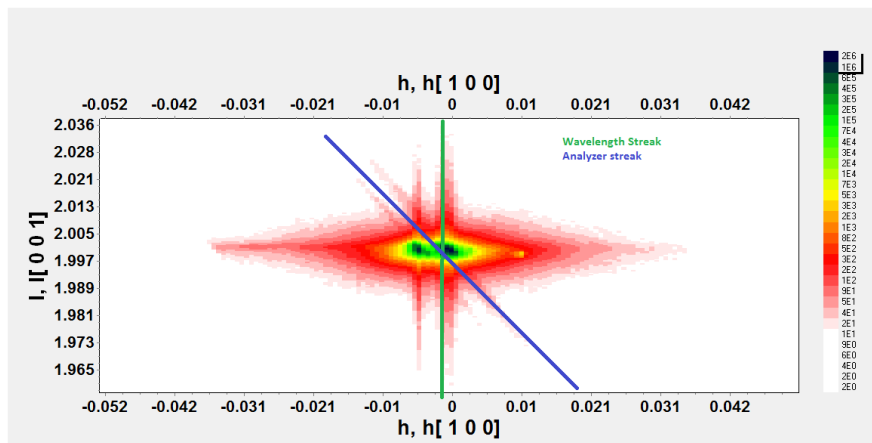

Fig.4.14.*RSM image around the (200) reflection of the STO(001) substrate treated at deposition conditions*

Though the map is expected to have a spherical distribution in 2D space some streaks are observed in the map which are represented by green and blue lines for the convenience of the reader. Such streaks arise from various sources and those details on the origin of streaks are given below:

Wavelength streak: A wavelength streak arise perpendicular to the surface of the sample as shown in the schematic figure 4.15. The minor wavelength spread which is inherent and theoretically Heisenbergs' uncertainty limit permits such deviation in the magnitude of wavelengths of atomic scale. Such deviation in the magnitude gives rise to a narrow distribution in the diffraction vector; effectively the Braggs condition is satisfied not at a point but over a narrow one dimensional distribution around a reciprocal lattice point. Hence, the reciprocal lattice point is actually observed as a 1D streak rather than a 0D spot. Thus in all RSM studies there exists a streak normal to the sample surface, which originates from the narrow distribution inherently present in the magnitude of the x-ray wavelength utilized.
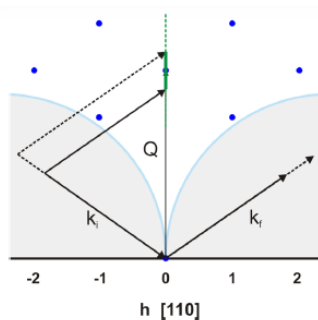

Figure 4.15: *Schematic explaining the origin of a wavelength streak normal to the surface of the sample.*

Analyzer streak: Due to the presence of an error function in an analyzer, streak forms along the direction of the scan. Figure.4.16 shows the red arc of scanning direction, the dark red line which is perpendicular to the diffracted wave vector is the trajectory of the analyzer streak.
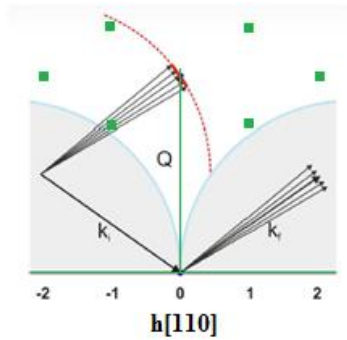
Fig 4.16 *Schematic explaining the origin of streak observed due to analyzer crystals.*

In addition to the analyzer and wavelength streak, a streak from the monochromator which is generally observed perpendicular to the incident wave and an additional streak arising from the instrument resolution function, which is observed along the geometric normal of the sample. In the symmetric scans, the wavelength streak and the instrument resolution streak coincides. Hence, elongation of intensity in different directions is observed in the RSM image of STO (001) (figure 4.14), however, only the wavelength streak and analyzer streak were observed and represented as blue and green line respectively.

In addition to the streaks, it is evident that the <002> orientation of STO exhibits a splitting adjacent to the main intense peak. Since a four bounce monochromator has been utilized the additional shoulder peak observed might not be due to the conventional $K_{\alpha 2}$ radiations. The shoulder peak associated with the 002 orientation is present with a miss orientation of angle 0.125°. Since the peak appears at a given 2 theta and with a variation in omega, it could be due to the presence of high miscut in the substrate, which is evident from the omega scan obtained from the RSM studies. It is also worth noting that such split was not observed when the diffraction information is collected in out of plane (Θ -2Θ scan) geometry. However, the miscut angle and other details remain ambiguous and a detailed analysis is needed.

(ii)   BCZT 600:

In order to confirm the epitaxial growth and cube on cube growth if any, the BCZT – 600 sample was scanned along (200) and (103) reflections. Figure4.17 shows the (200) reflection of BCZT-600.
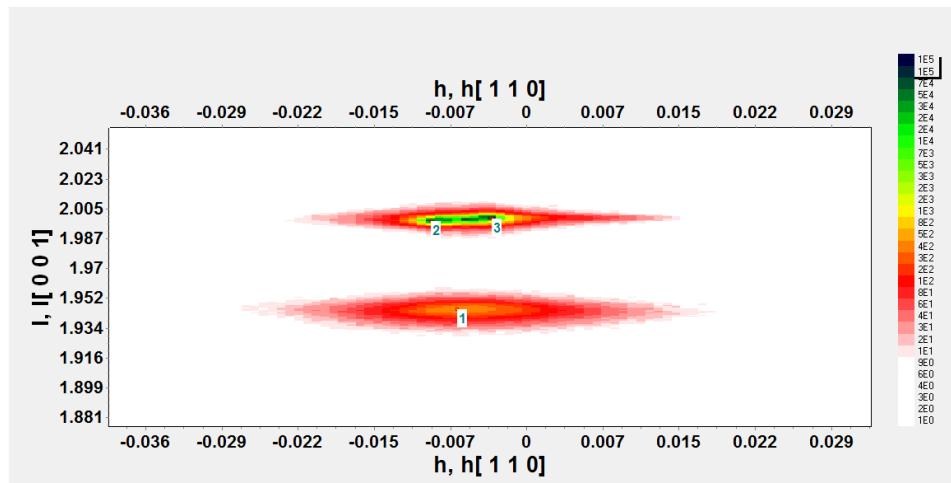
Fig.4.17 *reciprocal space map of BCZT-600 along (200)*

From the Fig 4.17 it is clear that the orientation of substrate and film are perfectly matches along the <110> direction. But, the area under projection of the film peak is broad and is as expected in the case of epitaxial thin films. The out of plane lattice parameter was found to be 4.016Å. Since in both the planar and the out of plane diffraction no orientation apart from (001) was detected, the film has grown epitaxially on the STO(001) substrate. Further analysis was performed in the asymmetric mode around (103) reflection by tilting the sample normal by 18.5°.The angle for the tilt is calculated by assuming a cubic growth and from the one third value of the out of plane lattice parameter. Figure.4.18 shows the RSM image of (103) reflection for BCZT-600.This picture confirms thought the film has taken the orientation of the substrate as a growth direction, no cube on cube growth is present and the film is completely relaxed. From the lateral lattice mismatch we could calculate the in plane lattice parameter of the film (4.0155). Hence we could conclude that BCZT-600 thin film has grown epitaxially on STO (001), but as a completely relaxed structure. The details of the relaxation are explained later.
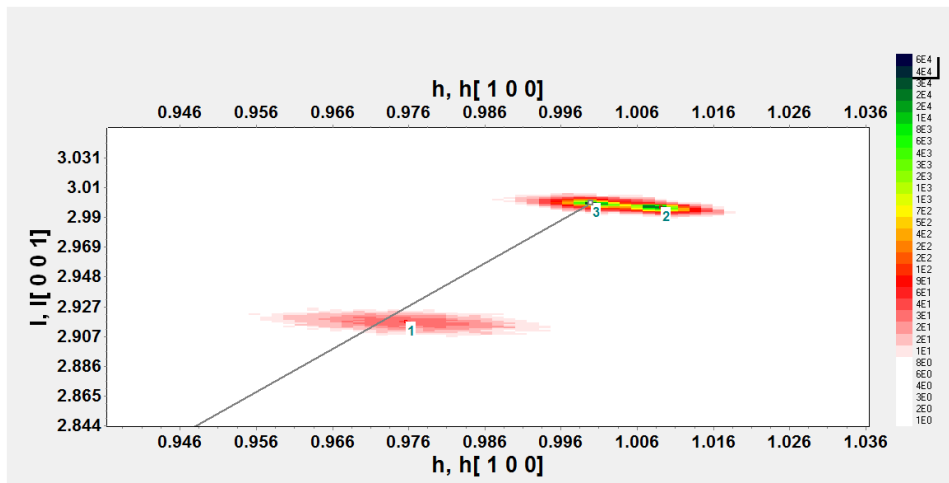
Fig 4.18R*eciprocal space map of BCZT-600 along (103)*

(iii) BCZT-650

RSM studies of BCZT-650 film confirm the epitaxial growth. Reciprocal space of (200) reflection was mapped with Θ - 2Θ geometry and omega relative start. Figure.4.19 shows the reciprocal space map of BCZT-650 sample along (200) reflection.
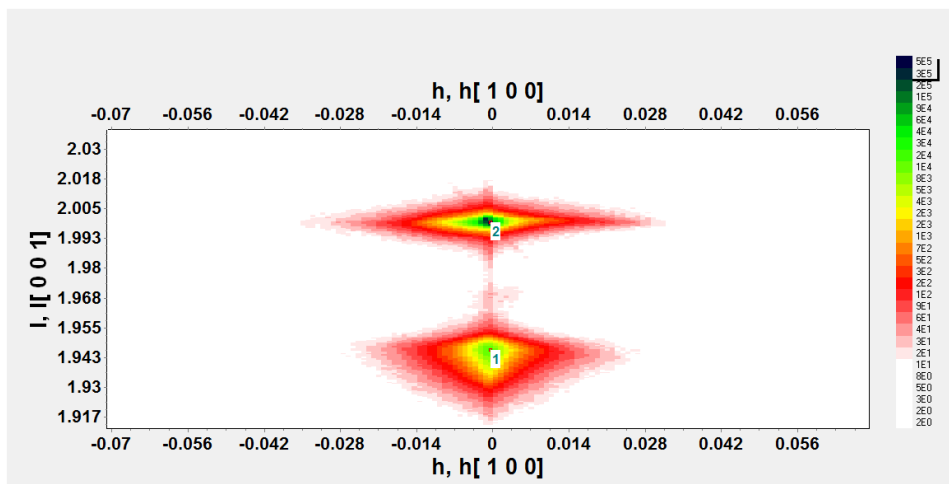

Fig 4.19 *RSM image of BCZT -650 along (200) reflection*

Out of plane Lattice parameter of BCZT film is found to be 4.0133Å and for substrate it is 3.9058Å, so the lattice mismatch is 2.74%. Further analysis of the film structure along (103) reflection was also performed. Fig.4.20 shows the RSM map of BCZT -650 sample along (103) reflection.
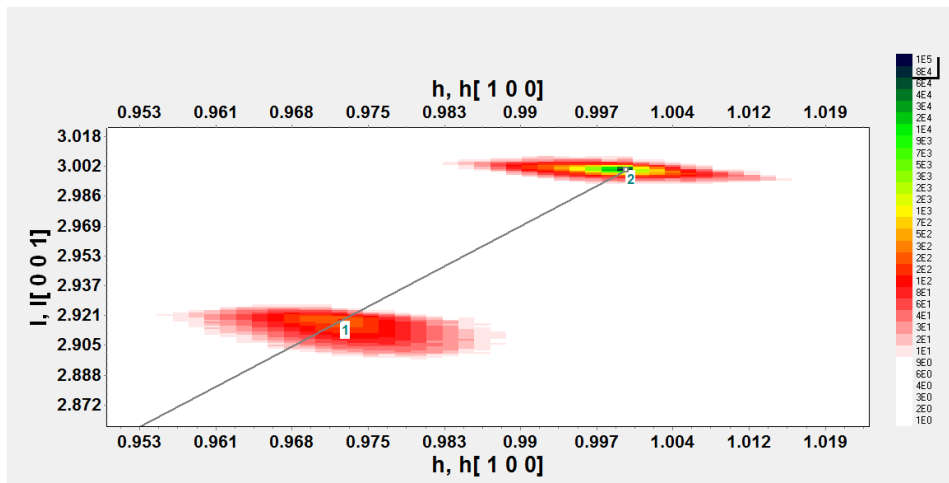
Fig 4.20*RSM image of BCZT-650 along (103) reflection*

Fig 4.20 confirms that the film is fully relaxed with the degree of relaxation (R= 0.9953).peak 1 in the picture shows BCZT film while 2 shows the substrate reflection. out of plane lattice mismatch with substrate is 0.0274, and the in plane lattice parameter of the film is found to be 4.0120, hence we got cube on cube geometry with the fully relaxed film.

(iv)   BCZT -675

Similar to the other RSM scans the BCZT-675 thin film was also scanned with the detector scan as shown in Figure 4.24. The RSM image of the BCZT-675 is shown below. The out of plane lattice parameter was found to be 4.011Å.
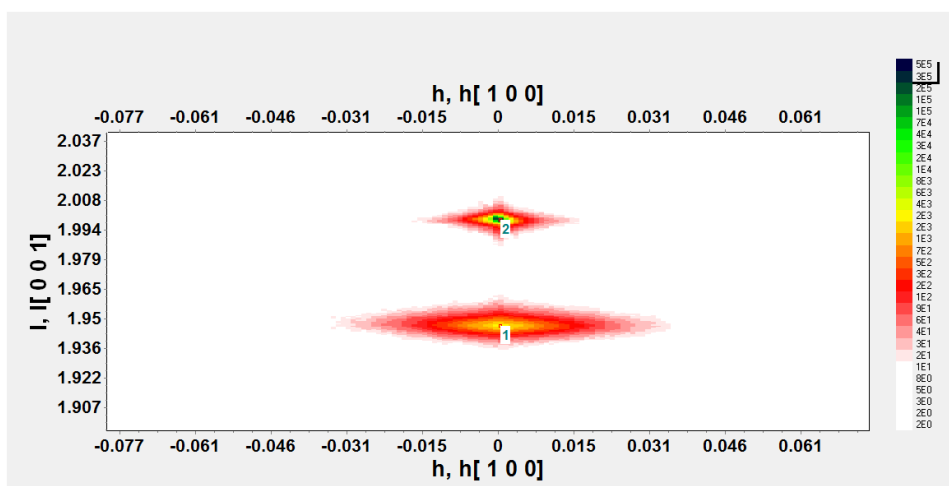

Fig 4.21*RSM image of BCZT-675 along (200) reflection*

4.2.8   Degree of relaxation in epitaxial thin films:

In epitaxial thin films the film is expected to be influenced by the substrate lattice parameter and hence, certain amount of strain is imparted into the lattice of the film from the substrate. Under such conditions, the film is said completely strained and as a result the in-plane lattice parameter of the film is expected to match with that of the substrate. However, the out of plane lattice parameter is also expected to undergo a compressive strain or a tensile strain if the in-plane lattice parameter experiences a tensile strain or a compressive strain respectively. Such a conjugative behavior is expected due to the elastic nature of the bonds that are present in the material of interest. However, beyond certain magnitude of strain and/or thickness the layer is expected to relax either completely or partially. The relaxation mechanism is widely studied and it is believed that the formation of misfit dislocations are one among the various route the strain relaxation takes place. RSM facilitates the researchers to identify if a film is completely and/or partially strained.
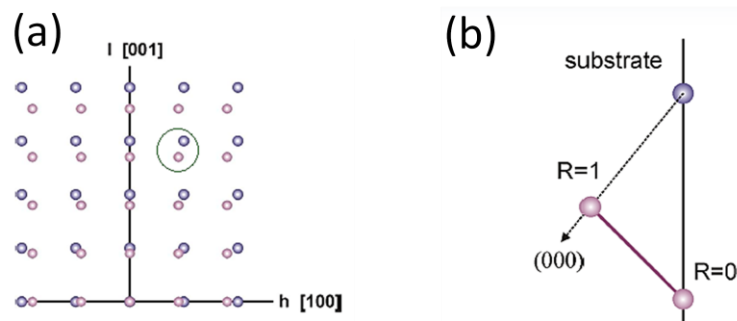

Fig 4.22 *(a) Schematic showing the reciprocal lattice points of both substrate and film in the case of strain relaxed thin films. (b) The schematic to explain the method of calculation of degree of relaxation*

As shown in the Fig 4.22 (a) the center of the peak position of both the film and substrate do not coincide in a given reciprocal lattice unit. In such cases, a triangle constituting the reciprocal lattice origin, peak center of the substrate and the film are constructed. The schematic Fig 4.22 (b) details the R=1 (completely relaxed) and R=0 (completely strained) conditions from the triangle.

$$\text{Degree of relaxation (R)} \quad = \quad \frac{Lateral\ lattice\ misatch}{relaxed\ lattice\ mismatch}$$

In our case the degree of relaxation for all the three samples were found to be close to 1, which indicates a complete strain relaxed growth, has taken place. Such a strain relaxed growth could be due to the larger thickness of the film (800-1000nm). In general, the epitaxial strain is expected to relax when the thickness of the films crosses 10-20nm based on the system and substrates.

In summary, all the BCZT films have grown phase pure on STO (001) substrates. It is also evident that the films have grown epitaxially in a complete strain relaxed fashion. However, since the morphological studies suggest the films grown at 650°C are suitable for further studies.

Chapter – 5

Summary and conclusions:

5.1   Summary:

In this thesis we have deposited epitaxial thin films of BCZT on STO (001) substrate. Substrate temperature was chosen from polycrystalline film data such that the recrystallized grains are deposited with relatively low defect densities (600°C,650°C, and 675°C). Detailed study on BCZT thin films for their morphology and structural characterization was carried out with AFM, SEM and HRXRD. In HRXRD studies,Θ - 2Θ scan was done to confirm the phase formation, Rocking curve analysis was carried out to check the mosaic character of deposited films, Reciprocal space mapping was performed to calculate the strain in the deposited films.

5.2   Conclusion:

- The growth of epitaxial thin films has been confirmed for all the substrate temperatures (600°C, 650°C and 675°C)

- Morphology studies confirmed that the film deposited at 650°C is having the least roughness value 4nm and better morphology among all the other films. It shows that at 650°C recrystallized grain growth has been taken place.

- From Θ - 2Θ scan phase purity was confirmed for the samples deposited at 600°C and 650°C, and 675°C

- Rocking curve analysis shows that film deposited at 650°C is having least mosaic structure (FWHM = 0.11) than the film deposited at 600°C (FWHM = 0.5) and 675°C(FWHM= 0.38)

- Reciprocal space mapping results shows that all the films are having completely relaxed growth with relaxation degree almost equal to 1, probably the high film thickness is the reason for the relaxed growth of the film.

- In plane and out of plane lattice parameters are found to be 4.0155Å and 4.016Å for film deposited at 600°C, 4.012 and 4.013Å for film deposited at 650°C and 4.011Å for film deposited at 675°C

5.3   Future Prospects:

As the epitaxial growth has been obtained for BCZT thin films on STO (100), it has been concluded that 650°C is the best temperature to grow epitaxial thin films, so following work can be done in future

- Deposition of BCZT on electrode material (SRO – Strontium Ruthenate) for investigation of piezoelectric response.
- Deposition of ultra-thin BCZT and study the effect of strain on the physical properties under strained conditions.

Reference:

[1]   Uchino, Kenji."Advanced Piezoelectric Materials."Science and Technolog (2010).

[2]   Lecture 18, "Properties of Materials" lecture slides (Aug 2013) – Dr. Ranjith
         Ramadurai-IIT Hyderabad

[3]   https://commons.wikimedia.org/wiki/File:Perovskite_ABO3.jpg

[4]   http://www.doitpoms.ac.uk/tlplib/piezoelectrics/pzt.php

[5]   B. Noheda, D. E. Cox, G. Shirane, J. A. Gonzalo, L. E. Cross, S. E. Park, Appl.
         Phys. Lett. **74**, (2059)

[6]   Wenfeng Liu1,Large Piezoelectric Effect in Pb-Free Ceramicsphysical review letter
         103, 257602 (2009)

[7]   Q.R. Lin, D.Y. Wang, Applied Surface Science **331,** 477–481(2015)

[8]   Milton Ohring, "Material Science of Thin films"(2nd edition) – wiley publication

[9]   Masashi Kawasaki, Atomic control of $SrTiO_3$ crystal surface, *Science,* 266 1540
         (1994)

[10]   M. Kareev, S. Prosandeep, Applied Physics Letters, **93,** 061909 (2008)

[11]   K. Szot, surface of reduced and oxidized $SrTiO_3$ from Atomic Microscopy, *Physical
         review,* **60**,5909(1999)

[12]   A. Biswas, Universal Ti termination of atomically flat $SrTiO_3$, *Applied physics
         Letter,* **98**, 051904 (2011)

[13]   A.VonHippel, Review of Modernphysics, **22,** 221 (1950)

[14]   Walter Heywang, Karl Lubitz, "Piezoelectricity" Springer series in Materials
         science

[15]   Introduction to solid state physics – Charles Kittel (wileyindia – 7th edition)

[16]   V.S. Tiwari, DhananjayaPandey, Physica B, **174,** 112 – 116 (1991)

[17]   Desheng Fu, Mitsuru Itoh and Shin-ya Koshihara, Applied Physics Letter,**93**, 012904 (2008)

[18]   Tsai-FaLin, Jien-LunLin, Chen-Ti Hu, Journal of Materials Science**26** ,491 496 (1991)

[19]   X.G.Tang, K.H. Chew, H.L.W. Chan, Acta Materialia, **52,** 5177–5183 (2004)

[20]   Dean S. Keeble, Feres Benabdallah, Applied Physics Letters,**102**, 092903 (2013)

[21]   David W. Hoffman and Robert C. McCune, Microstructural Control of Plasma-Sputtered Refractory Coatings, Handbook of Plasma Processing Technology,

[22]   Prabaharkutty et.al, Thin solid films, *Manuscript under review*

[23]   G. Bauer, J.H. Li,Acta physica polonica*A Vol. 89,* no. 2 *(1996)*

[24]   www.bruker-webinars.com (Dr. Martin Zimmermann- lecture on HRXRD- 24th march 2011)